IEEE Access
Multidisciplinary ⋮ Rapid Review ⋮ Open Access Journal

Received October 23, 2020, accepted October 28, 2020, date of publication November 2, 2020, date of current version November 25, 2020.

*Digital Object Identifier 10.1109/ACCESS.2020.3035317*

# Combined Ray-Tracing/FDTD and Network Planner Methods for the Design of Massive MIMO Networks

**MICHEL MATALATALA TAMASALA[1], SERGEI SHIKHANTSOV[1], MARGOT DERUYCK[1], EMMERIC TANGHE[1], (Member, IEEE), DAVID PLETS[1], (Member, IEEE), SOTIRIOS K. GOUDOS[2], (Senior Member, IEEE), LUC MARTENS[1], (Member, IEEE), AND WOUT JOSEPH[1], (Senior Member, IEEE)**

[1]Department of Information Technology, Ghent University/IMEC, 9052 Ghent, Belgium
[2]Department of Physics, Aristotle University of Thessaloniki, 54124 Thessaloniki, Greece

Corresponding author: Michel Matalatala Tamasala (michel.matalatala@ugent.be)

This work was supported by the Research Foundation at UGent (BOF-UGent) under Agreement 01W0014.

**ABSTRACT** The design of a massive MIMO network requires a channel model that captures the Spatio-temporal dimensions of the propagation environment. In this paper, we propose a novel method combining Hybrid Raytracing - Finite difference time domain (FDTD) and network planner tools to address this requirement. This method provides accurate and realistic EMF exposure models for the design of a massive MIMO network. Using this method, we proceed with the optimization of the BS's locations under the low power consumption and low EMF exposure constraints. Assuming equal preference of the optimization objectives, the simulations show that the uplink localized 10g dose appears to be the dominant factor of the localized 10g EMF exposure. Moreover, a massive MIMO network designed to serve 224 simultaneous active users at the same time-frequency resource is subject to an increase of the total whole-body dose (2 times higher in downlink and +18% in uplink), compared to a design with 14 active users. However, in the same conditions, the downlink localized 10g dose reduces (20 times lower) whereas the uplink localized 10g dose increases (+23%) in comparison with the scenario with fewer users (14). Besides, the electromagnetic field strength in all locations obtained with this new method is 2 times weaker compared to a 4G LTE network, while complying with the international guidelines.

**INDEX TERMS** 5G, antenna arrays, beamforming, EMF exposure, massive MIMO, power consumption, network planner, precoding, ray-tracing.

## I. INTRODUCTION

Massive Multiple Input Multiple Output (mMIMO) is expected to be used in the fifth generation wireless communications (5G) and enables the possibility for the operators to deploy and run a network that is both spectral and energy efficient, while delivering unprecedented capacity to the users. The massive MIMO (mMIMO) key enabler allows the 5G base station (BS) to focus the antennas' energy towards the direction of the intended user while suppressing the interference from the other users by utilizing beamforming in line-of-sight situation (LOS) or precoding in non line-of-sight (NLOS). This leads to spatial concentration of peaks of power density around the users and may result into a significant level of electromagnetic (EMF) exposure [1]. This needs to be taken into account for the design of the mMIMO cellular networks, in addition to the power consumption of the network.

Designing a mMIMO network requires good knowledge of the environment in which the network is deployed as the propagation paths are affected by the presence of buildings and other obstacles, which modify the characteristics of the propagation. Accurate modeling is needed to capture the contributions of all the propagation paths through some physical characteristics at the receiver side such as the direction of arrival (DoA), the direction of departure (DoD), the power and time-delay of each incident ray. The straightforward way to characterize wireless propagation in network design is the

The associate editor coordinating the review of this manuscript and approving it for publication was Fan-Hsun Tseng.

use of the theoretical models (Friis model) and the empirical wave propagation models that are strictly dependent on the environment of study [2], [3]. However, both the theoretical and the empirical models do not render accurate information related to the spatial consistency required for mMIMO channels to account for the variation of the large-scale and small-scale fading parameters with the user equipment (UE) locations [2], [4].

Recently, the ray-tracing (RT) method has been widely adopted to estimate the channel characteristics within an indoor or outdoor propagation environment, embedding the directional information through the propagation rays, such as the angle of arrival/departure, the path loss, and the time delays [1], [2], [4], [5]. Rather than providing approximate formulas developed based on field measurements in specific environments used by the empirical models, the RT aims at modeling the propagation of EM waves accounting for the specificity of a particular physical environment such as the directional information from multi-path components due to the presence of obstacles and the correlations between the antenna elements of the base stations [6]. The use of the RT is beneficial for the wireless network planning since it helps obtaining a realistic evaluation of the level of EMF exposure due to the transmission of the base stations in terms of electric field (E-field) or specific absorption rate (SAR) which encompasses the whole-body ($SAR_{wb}$) and the peak-spatial localized SAR (psSAR). In this paper, we design optimal mMIMO networks by optimizing the positions and the power levels of the BSs with respect to the low power consumption and the low level of EMF exposure requirements. To achieve this, the RT method is combined with the capacity-based network deployment tool of [7] to proceed with the joint optimization of mMIMO networks. It is worth noting that the computation of the psSAR requires the finite difference time domain (FDTD) method to be combined with the RT as proposed in [1]. The output of the RT simulation (Poynting vector and psSAR) will then be used by the capacity-based network tool for optimization purposes. The details of this process will be provided further in this paper.

Other related works have dealt with the investigation of EMF exposure due to the transmission of mMIMO base stations [1], [5], [6], [8]–[10]. In [1], the authors resorted to a numerical method, combining ray-tracing and FDTD simulations to estimate realistic levels of mMIMO EMF exposure. The investigation carried out in [5] utilizes the same method (combined RT-FDTD) for the modeling of mMIMO propagation channel, accounting for the user-induced coupling effects. The authors of [8] used stochastic channel models to show that the mMIMO BS realistic power levels yielding to an accurate EMF assessment is found to be less than 15% of the corresponding theoretical maximum power. In [6], the authors analyzed the performance of a 16-BS mMIMO network by means of an RT-based deterministic tool and noticed a significant difference in terms of throughput statistics while using various type of array configurations. The work of [9] developed an open-source system level simulator for the design of spectral and energy efficient mMIMO systems based on statistical channel models to optimize the spectral and energy efficiency. In [10], the authors proposed the best practices guiding the planning of 5G networks under EMF constraints. However, none of the related works addressed mMIMO network design by joint optimization of the BS placement and power levels towards minimal power consumption and minimal EMF exposure, using a combined ray-tracing network planner method. The main contributions of our study are the following:

- Optimizing the mMIMO BSs' locations under realistic EMF exposure constraints (E-field) obtained with the RT method, accounting for the directional information per BS antenna element (AoA, AoD, time delays, spatial consistency) and the inter-antenna correlation. The use of a hybrid RT-based propagation model provides a more accuracy network planning compared to the empirical models as the spatial and time domain requirements of mMIMO are addressed.
- Addressing the localized SAR (psSAR) due to mMIMO BS downlink in addition to the whole-body SAR in the optimization process, using the hybrid RT-FDTD method. To the best of our knowledge, this is the first time the 10g localized SAR due to BS ( [1]) is considered in mMIMO network planning.
- Realistic estimation of the beamforming gain and precoding based on the propagation characteristics provided by the ray optics rather than considering the theoretical values.

Table 1 outlines the contributions of this work with respect to the other related relevant papers in the literature.

The remainder of this paper is organized as follows: Section II explains the method pursued to combine the ray-tracing, the FDTD, and the capacity-based network deployment tools. Section III presents and discusses the main results of the simulations before concluding the study in Section IV.

## II. METHOD

This section focuses on the numerical approach and explains in details the different steps for designing the mMIMO network based on low power consumption and EMF exposure. The method consists of three main blocks as depicted in Fig. 1: the Ray-tracing simulator (left), the FDTD simulator (middle) and the capacity-based network deployment tool (right).

### A. ENVIRONMENT OF STUDY

The environment of deployment of mMIMO BSs is based on the 3D geographical system information (GIS) which is related to a 6.85 $km^2$ suburban area in Ghent, Belgium. This area is covered by 75 4G BSs in order to provide voice and data services to the users. The same environment is used for both the RT-FDTD and the optimization simulations. The mMIMO BSs deployed in the environment have a total

**TABLE 1. Work positioning with respect to the other relevant papers in the literature.**

| Work | Objective | Main parameter investigated | Method | EMF Regulations | Contributions |
|---|---|---|---|---|---|
| This work | mMIMO 5G networks design under power consumption and EMF constraints | - Power consumption<br>- DL EMF exposure : Whole-body and localized 10g dose<br>- UL EMF exposure: whole-body and localized 10g dose | Combined RayTracing-FDFD/Network planning methods, heuristic | ICNIRP-based | - Optimize mMIMO BSs' locations and power under realistic EMF constraints obtained with RT method.<br>- Accounting for localized 10g psSAR due to mMIMO precoding during optimization process.<br>- Realistic estimation of BF (precoding) gain based on ray optics rather then theoritical values. |
| [1] | Estimate realistic level of mMIMO exposure | $\mathrm{pSAR}_{10g}$ due to precoding in DL | Combined RT-FDTD | ICNIRP-based | First evaluation of $\mathrm{pSAR}_{10g}$ due to mMIMO BS precoding in DL. |
| [2] | Radio propagation modeling using RT methods | RT algorithms review | Ray-tracing | Not covered | Discuss RT methods accuracy and computation speed. |
| [3] | Radio propagation modeling for 5G networks in the mm-wave spectrum | - Large scale fading<br>- Empirical path loss models | In situ measurements at 28 and 38 GHz in New york city and Austin | Not covered | Develop empirical path loss models for 5G networks in the mm-wave spectrum, based on the propagation data measured. |
| [4] | Channel modeling at mm-wave | 3D-based multipath channel parameters for spatial consistency | millimeter-wave channels simulator | Not covered | Account for spatial consistency in mm-wave channels simulator. |
| [5] | mMIMO propagation channel modeling | User induced coupling effects in mMIMO channel modeling | Combined RT-FDTD | ICNIRP-based | Fisrt time user induced coupling effects accounted for in 5G mMIMO channel modeling. |
| [6] | Evaluation of a large-scale multi-cell mMIMO network | Impact of array configuration on throughput statistics | - Ray-based deterministic tool<br>- Theoretical Rayleigh fading channel model | Not covered | Demonstrate the performance of practical mMIMO systems in real propagation conditions. |
| [7] | Optimal low-power design of 5G mMIMO networks | mMIMO performance evaluation | Network planning methods, heuristic | not covered | Optimize mMIMO BSs' locations and power levels under power consumption constraints using empirical PL model. |
| [8] | Estimate realistic level of mMIMO exposure | Time-averaged realistic maximum power level of 5G BS | Statistical methods | ICNIRP-based | The largest realistic maximum power level was found to be less than 15% of the corresponding theoretical maximum. |
| [9] | Optimization of the spectral and energy efficiency of mMIMO systems | spectral and energy efficiency | system level simulator | Not covered | Realistic assessment of spectral and energy efficiency. |
| [10] | Planning of 5G networks under EMF constraints | Throughput, minimum signal- to-interference ratio (SIR), threshold, maximum coverage distance | Linear programming optimization model, heuristic | Strict EMF limits | - Use of temporal and statistical models (with parametrs variation) for EMF evaluation<br>- Consider heterogeneous 5G network consisting of micro and macro gNode BSs. |

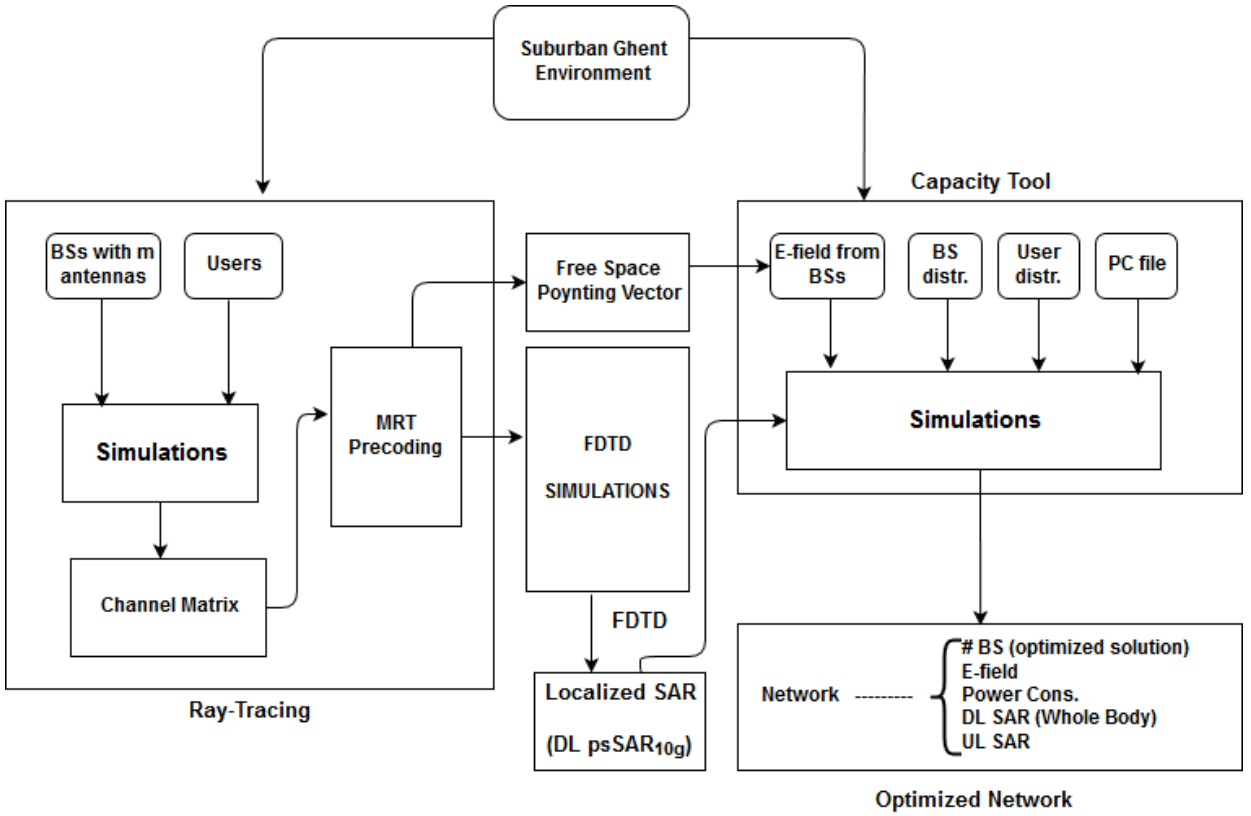


**FIGURE 1. Optimization block-diagram showing the Ray-tracing (left), FDTD (middle) and capacity-based network simulator (right).**

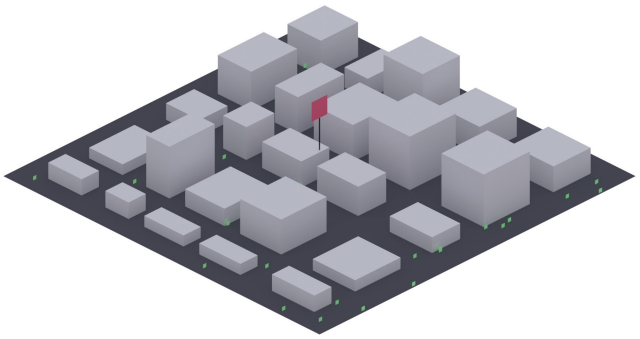

**FIGURE 2.** The outdoor urban environment sample model considered for the computation in the RT-FDTD tool. Cuboid buildings are distributed on a rectangular grid covering a 200 m by 200 m area.The mMIMO BS (shown in red) is positioned in the area center at the fixed 35 m height. 50 users (shown in green) are distributed randomly outdoors.

transmit power fixed at 43 dBm [11] and are equipped with 100 antenna elements operating at 3.5 GHz with 20 MHz bandwidth, arranged in a 10 x 10 array. The other radio link parameters like the antenna gains, the signal to noise ratio (SNR), the feeder loss and the noise figure needed for the evaluation of the link budget are obtained as in [12]. The user equipment (UE) consists of a single omni-directional antenna.

### B. RAY-TRACING AND FDTD

We make use of the hybrid ray-tracing FDTD tool as proposed in [1], [5], [13] for more accurate estimation of the propagation characteristics of the EMF signal within the area of a mMIMO network deployment. The estimation of a channel with the RT method includes all the propagation mechanisms that may affect the EMF signal during its trip to the end-user: reflections, transmissions and diffraction [1]. While FDTD is applied to the areas close to the user equipment (UE) with complex discontinuities, the RT is considered to analyze and simulate the propagation of EMF waves in a wider outdoor environment including buildings with different heights, ranging from 2.5 to 114.5 m.

Given the complexity of the environment described above, that would require high computational time, we model an environment sample with respect to site-specific accurate information related to the buildings features like heights, wall locations, building materials, side lengths, spacing, etc. The environment sample models a single outdoor urban macro-cell. The area is a square with a 200 m side length. It consists of a flat ground-plane and cuboid building blocks as shown in Fig 2. The buildings' size and position are determined using stochastic geometry approach according to the following rule, accounting for city properties of Ghent:

- Building blocks are modeled as cuboids arranged on a rectilinear xy-grid.
- The block height has a uniform random distribution from 10 m to 30 m.
- The block side length has a uniform random distribution from 10 m to 30 m.
- The distance between blocks in the x and y direction in sampled independently with equal probability from the 10 m, 15 m, 20 m discrete set.

A single BS is located at a fixed height of 35 m at the center of the xy-plane (Fig. 2). It is equipped with 100 dipole antenna elements, arranged in a 10-by-10 square array with a half-wavelength spacing at the center frequency of 3.5 GHz. This spacing setup corresponds to the first minimum distance that ensures a lower correlation between antenna elements [14] and meets the real-life applications that are space-constrained. The users (50) are static and randomly distributed in the area. The location of the BS is such that the area of interest is fully covered with some users having LOS to the BS and others in NLOS (green squares in Fig. 2). The latter case is due to the presence of buildings that obstruct the signals towards those users. This environment model makes it possible to acquire realistic variable channel predictions needed for the mMIMO study.

The RT simulations (Fig. 1, left) are performed with the Wireless InSite 3.2 (REMCOM) software suite. Based on the software input consisting of the physical environment, the location of the users and the number of BS antenna elements, the software pre-computes the mMIMO channel between each antenna element of the BS and the users and creates channel matrices with all BS-user combinations from the pre-computed data. The combination between an $m^{th}$ antenna of the mMIMO BS and a $k^{th}$ UE is denoted a path, described by its complex-valued impulse response $\delta$ and time-delay $\tau$ [1], [6]. Then, the RT simulations is run, including the linear precoding schemes, inherent to mMIMO operation. The maximum ratio transmission (MRT) scheme has been used in this study. The complex-valued propagation channel $h_m^k$ between each pair of $m^{th}$ BS antenna element and $k^{th}$ user is given as follows [1]:

$$h_k^m = \sum_{l=1}^{s(k,m)} \delta_l \, exp\,(-2\pi \; if_c\tau_l) \tag{1}$$

With $\delta_l$ the complex-valued impulse response towards the $l^{th}$ path between the $m^{th}$ antenna element and the $k^{th}$ UE; $\tau_l$ the time-delay recorded on the $l^{th}$ path and $s(k;m)$ the number of paths between the $m^{th}$ antenna element and the $k^{th}$ UE; $f_c$ the operating frequency. The corresponding channel matrix $G(f_c)$ is obtained by the Fourier transform of (1) at the carrier frequency of 3.5 GHz at which the mMIMO BS is operating.

The RT is combined with the FDTD method (Fig. 1, middle) in this study to investigate the level of EMF exposure in the neighborhood of the UE. To achieve this, the EM-FDTD solver of Sim4Life v4.0 (ZMT, Zürich, Switzerland) has been used for the simulations in which the plane wave source of EMF has been modeled by an incident ray whose impulse response is proposed in Eq. 1. The EMF-exposure is assessed with the ViP v.3.1 Duke heterogeneous human phantom [1]. Since incident rays emanate from each antenna element, the higher the number of antenna elements used at the BS, the higher the number of incident rays to be handled in

the FDTD software, and the higher the simulation time. The authors in [1] showed that an average of 220 rays observed at each TX-RX pair led to 8,103 incident rays at the UE side, which is huge to process. They resorted to the directional of arrival (DoA)'s discretization to overcome this constraint, consisting in adding up the incident rays with almost equal DoA values. This results in a reduction of the FDTD simulations run-time by a factor of 30 (around 3 hours per simulation on a common desktop personal computer (PC) with Intel i5 5$^{th}$ generation CPU and Nvidia GTX 1050 Ti graphic card - GPU). The error introduced by this approximation was investigated and reported to be acceptable [1]. The same approach is considered here.

Considering the channel matrix element proposed in Eq.1, the complex amplitude of the E-field of the $l^{th}$ ray incident from the $m^{th}$ BS antenna element at the $k^{th}$ user, using the MRT precoding is obtained as follows [1]:

$$\hat{\boldsymbol{E}}^{l}_{k,m} = \boldsymbol{E}^{l}_{k,m}\, exp\,(-i\, arg\,(h^{m}_{k})) \tag{2}$$

Similarly, the magnetic H-field is defined as follows [1]:

$$\hat{\boldsymbol{H}}^{l}_{k,m} = \boldsymbol{H}^{l}_{k,m}\, exp\,(-i\, arg\,(h^{m}_{k})) \tag{3}$$

With both $\boldsymbol{E}^{l}_{k,m}$ and $\boldsymbol{H}^{l}_{k,m}$ the E-field and H-field amplitudes, respectively.

Based on (2) and (3), the E-field and the H-field at a distance r to the proximity of the $k^{th}$ user are obtained as the sum over all rays and the M BS antenna elements, respectively:

$$\boldsymbol{E}^{MRT}_{k}(\boldsymbol{r}) = \sum_{m=1}^{M}\sum_{l}\hat{\boldsymbol{E}}^{l}_{k,m}\, exp\,(-i\,\boldsymbol{k}_{l}\cdot\boldsymbol{r}) \tag{4}$$

$$\boldsymbol{H}^{MRT}_{k}(\boldsymbol{r}) = \sum_{m=1}^{M}\sum_{l}\hat{\boldsymbol{H}}^{l}_{k,m}\, exp\,(-i\,\boldsymbol{k}_{l}\cdot\boldsymbol{r}) \tag{5}$$

where $\boldsymbol{r}$ denotes the distance vector between the BS and the $k^{th}$ user and $\boldsymbol{k}_l$ refers to the wave-vector associated to the $l^{th}$ ray.

Then, the time-averaged radiated EMF energy is obtained as the real part of the Poynting vector [1], [15]:

$$\boldsymbol{S}^{MRT}_{k}(\boldsymbol{r}) = \frac{1}{2}\boldsymbol{Re}[\boldsymbol{E}^{MRT}_{k}(\boldsymbol{r}) \times \boldsymbol{H}^{*MRT}_{k}(\boldsymbol{r})] \tag{6}$$

where $\boldsymbol{H}^{*MRT}_{k}$ and $\boldsymbol{E}^{MRT}_{k}$ are the complex-conjugated magnetic field and the electric field at the vicinity of the user $k$, respectively.

The values of the magnitude of the Poynting vector and the electric-field (E-field) one are computed from the simulations over 100 samples of LOS/NLOS environments in order to obtain results with good agreement. The 25$^{th}$ and 75$^{th}$ percentiles over the 100 samples have been considered. Further in the paper, we utilize the power density obtained in (6) for the computation of the whole-body SAR to be used in the optimization tool (Fig. 1, right). At the same time, the precoded rays resulting from the precoding matrix are used as excitation of the EMF sources for the simulations in the FDTD tool. This latter provides the level of localized EMF exposure in terms of peak-spatial SAR averaged over 10g of tissue psSAR10g. Regarding the simulations of the FDTD, the ViP v.3.1 Duke heterogeneous human phantom of [16] has been used to evaluate the level of EMF-exposure, with the position of the UE located close to the head.

### C. PROBLEM DESCRIPTION

In this study, we optimize the placement and the power levels of the mMIMO BSs in a suburban Ghent area using the mMIMO network planner (Fig. 1, right block). The problem consists in guaranteeing both the maximum area coverage and the maximum user coverage, while simultaneously minimizing the power consumption of the entire network, the downlink exposure due to the BSs and the uplink exposure resulting from the transmission of the users. It's worth mentioning here that only the users are considered for the beamforming/precoding of the mMIMO; the non users and by-standers are not taken into account. This problem is similar to the one investigated in [12]. However, here, the RT-FDTD prediction tool (left and middle blocks of Fig. 1) is used to account for the spatial consistency requirement of the mMIMO. The outputs of the RT-FDTD tool (E-field and localized psSAR$_{10g}$) are injected in the network planner tool (right block of Fig. 1) for optimization process purposes.

Assuming that a mMIMO based mobile network consists of $N$ BSs and $K$ users, we define $\mathcal{K} = \{1, 2, \cdots, K\}$ and $\mathcal{N} = \{1, 2, \cdots, N\}$, to be the sets of users and BSs, respectively. The number of users assumed in this study (from daily hourly traffic) and the initial set of BSs (75 BSs) have been provided by a Belgian mobile operator. Furthermore, the set of power values of each BS is denoted as follows: $\mathcal{P} = \{p_1, p_2, \cdots, p_n\}$. Let $x_{kn}$ be the binary variable indicating the association of the $k^{th}$ user with the $n^{th}$ BS and can be formulated as

$$x_{kn} = \begin{cases} 1, & \text{if } k\text{-th user is associated with the } n\text{-th BS} \\ 0, & \text{otherwise.} \end{cases} \tag{7}$$

Similarly, the binary variable $y_n$ describes the operation or not of the $n$-th BS and can be defined as

$$y_n = \begin{cases} 1, & \text{if BS n is turned on} \\ 0, & \text{otherwise.} \end{cases} \tag{8}$$

Additionally, we can define the discrete variable, $p_n$ that describes the transmission power value of the $n$-th BS as $p_n \in \{0, 1, 2, \cdots, p_t\}, \forall n \in \mathcal{N}$. Where $p_t$ is the maximum allowable transmission power for a BS according to 3GPP recommendations ($p_t = 43$ dBm in this work). Thus, we define the solution vector to an integer vector that contains the active or not BSs, the operating power in dBm and the users associated.

### D. OBJECTIVE FUNCTIONS

Here, we proceed with the mMIMO network joint optimization towards the power consumption and the EMF exposure which consists of the whole-body downlink exposure,

the whole-body uplink exposure, the localized downlink exposure and the localized uplink exposure. To achieve this, we define useful metrics needed for the optimization process: the power consumption (P), the whole-body downlink dose ($D_{wb}^{DL}$), the whole-body uplink dose ($D_{wb}^{UL}$), the downlink localized 10g dose ($D_{10g}^{DL}$) and the uplink localized 10g dose ($D_{10g}^{UL}$). These metrics are linearly combined using the weighing vector to form a utility function denoted fitness function [17], which is expressed as follows:

$$F = \sum_{i=1}^{3} \omega_i \cdot f_i(P, D_{wb}, D_{10g}) \tag{9}$$

With F the utility function denoted fitness function, $\omega_i$ ($0 \leq \omega_i \leq 1, i = 1, 2, 3$) the weighing depending on the priority towards either objective considered [18], [19]. $f_i(P, D_{wb}, D_{10g})$ is a function of the power consumption P ($i = 1$), the whole-body dose ($D_{wb}$, $i = 2$) and the localized 10g dose ($D_{10g}$, $i = 3$), respectively.

### 1) POWER CONSUMPTION OBJECTIVE FUNCTION

The power consumption objective function is defined as follows:

$$f_1 = 1 - \frac{\sum_{n \in \mathcal{N}} P_{des}(y_n p_n)}{P_{max}} \tag{10}$$

where $P_{des}()$ refers to the power consumption of the designed network in W and computed similarly to [20]–[22]; $P_{max} = N \times P_{des}(p_t)$ is the maximum power consumed (in W) by the entire network when all BSs are assumed active and transmitting at maximum power (43 dBm). The values of $p_n$ expressed in dBm have to be converted in W prior to proceed with the calculation of the power consumption.

### 2) EMF EXPOSURE OBJECTIVE FUNCTION

The EMF exposure objective function is defined in terms of total whole-body dose and total localized 10g dose. For simplicity, it is assumed that the absorbed energy is summed at the same location: any location of the human body for the whole-body EMF exposure and the human brain tissue for the localized 10g EMF exposure. In this study, the investigation of the EMF exposure does not account for the bystanders and the other users [23].

1) Total whole-body Dose
The whole-body dose function is defined as follows:

$$f_2 = 1 - \frac{\underset{n \in \mathcal{N}}{D_{wb}(y_n p_n)}}{{D_{wb}}^{max}} \tag{11}$$

With $\underset{n \in \mathcal{N}}{D_{wb}()}$ (J/Kg) the global EMF exposure metric in terms of total whole-body dose due to the traffic of all the active BSs and the UEs covered by the network, obtained as an average of the $50^{th}$-percentile and the $95^{th}$-percentile of the individual whole-body doses [19]; $D_{wb}^{max}(\frac{J}{Kg})$ the total whole-body dose due to the traffic of the entire network when assuming all the BSs are active and working with the maximum antenna array configuration and all UEs are covered.
The total whole-body dose $D_{wb}$ is computed as the sum of the downlink whole-body dose ($D_{wb}^{DL}$ [J/Kg]) due to the transmission of the BSs and the uplink whole-body dose (($D_{wb}^{UL}$ [J/Kg])) due to the transmission of the UEs and the uplink whole-body dose due to the transmission of the UEs ($D_{wb}^{UL}$ [J/Kg]):

$$D_{wb} = D_{wb}^{DL} + D_{wb}^{UL} \tag{12}$$

Each of these absorbed doses is obtained by multiplying the corresponding SAR value with the duration of the exposure as follows:

- Whole-body Downlink dose ($D_{wb}^{DL}$):
The following formula is used [24]:

$$D_{wb}^{DL} = T^{DL} \cdot SAR_{wb}^{DL} \tag{13}$$

With $T^{DL}$ the duration of the exposure in [s], set to 3600 s, since the number of the users considered in this study derives from the hourly traffic of a Belgian mobile operator in Ghent [12] and $SAR_{wb}^{DL}$ [W/Kg] the whole-body SAR due to downlink and calculated as follows:

$$SAR_{wb}^{DL} = \sum_{BS_{n,k}} (S_{BS_{n,k}} \cdot SAR_{REF_{wb}}^{DL}) \tag{14}$$

$SARDL_{REF_{wb}}^{DL}$ is the reference whole-body SAR for 1 [W/m$^2$] of received power density [24] and $\sum_{BS_{n,k}} S_{BS_{n,k}}$ is the power density due to the transmission of all the active BSs to the user k, obtained with the RT-FDTD simulation tool (Fig. 1, left) as proposed in Eq. 6. This is the sum of the individual power densities due to the serving BS and the other neighboring BSs contributing to the EMF exposure at the user's location [12], [25].
- Whole-body uplink dose ($D_{wb}^{UL}$ [J/Kg])
The whole-body uplink dose $D_{wb}^{UL}$ [J/Kg] is triggered by the transmission of the UEs towards the base station. It is expressed as follows [24]:

$$D_{wb}^{UL} = T^{UL} \cdot SAR_{wb}^{UL} \tag{15}$$

With $SAR_{wb}^{UL}$ the whole-body uplink SAR obtained with the below equation:

$$SAR_{wb}^{UL} = P_{act} \cdot DC_{TDD}^{UL} \cdot SAR_{ref}^{UL} \tag{16}$$

where $DC_{TDD}^{UL}$ ( $= 25\%$ [8]) denotes the uplink duty cycle inherent to the TDD mode of the operation assumed for the mMIMO network. $SAR_{ref}^{UL}$ refers to the reference whole-body uplink SAR in [W/Kg] for 1 W of transmitted power ($SAR_{ref}^{UL} = 0.0052$ [W/Kg]), obtained by simulations using the FDTD numerical tool (Sim4life) with a dipole at 3.5 GHz, positioned next to the

right ear. $P_{act}$ [W] accounts for the actual transmission power from the UE obtained as follows:

$$P_{act}[dBm] = \min(RXsens + PL, 23) \quad (17)$$

with

$$RXsens = 10\ \log_{10}\ (K \cdot T \cdot B) + NF + SNR \quad (18)$$

RXsens refers to the receive sensitivity of the BS; K is the Boltzmann constant ($1.38 \cdot 10^{-23}$ [J/K]); T (= 290 K) is the temperature in Kelvin; B (= 20 MHz) is the bandwidth; NF [dB] is the noise figure; SNR [dB] is the signal to noise ratio and PL [dB] stands for the propagation path loss between the BS and the user. The number 23 in Eq. 17 refers to the maximum output power of the 5G user's device in dBm [26]. The total whole-body uplink dose of the entire network is obtained by the average of the $50^{th}$-percentile and the $95^{th}$-percentile of the individual whole-body uplink doses.

2) Total localized 10g dose ($D_{10g}$ [J/Kg])
The total localized 10g dose function is defined as follows:

$$f_3 = 1 - \frac{\sum\limits_{n \in \mathcal{N}} D_{10g}\,(y_n p_n)}{D_{10g}^{max}} \quad (19)$$

With $\sum\limits_{n \in \mathcal{N}} D_{10g}(\,)\ (\frac{J}{Kg})$ the total localized 10g dose due to the traffic of all the active BSs and the UEs covered by the network:

$$D_{10g} = D_{10g}^{DL} + D_{10g}^{UL} \quad (20)$$

$D_{10g}^{max}(\frac{J}{Kg})$ is the maximum total localized 10g dose resulting from the traffic of the entire network when assuming all the BSs are active and working with the maximum antenna array configuration and all UEs are covered; $D_{10g}^{DL}$ [J/Kg] is the total downlink localized 10g dose due to the beamforming or precoding that focuses EMF energy to the intended users [1], [5] and $D_{10g}^{UL}$ [J/Kg] is the total localized 10g dose resulting from the transmission of the covered UEs. The global values of both the $D_{10g}^{DL}$ and the $D_{10g}^{UL}$ are obtained by the average between the $50^{th}$-percentile and the $95^{th}$-percentile of the corresponding individual 10g doses.

- Downlink localized 10g dose ($D_{10g}^{DL}$ [J/Kg]) [1], [5]
During the operation of a mMIMO BS, the use of beamforming or precoding helps focusing the EMF signal in the direction of the intended user. The localized EMF exposure resulting from this highly focused energy has been addressed in [1] in terms of $psSAR_{10g}$ and the related dose is expressed as follows:

$$D_{10g}^{DL} = T^{DL} \cdot psSAR_{10g}^{DL} \quad (21)$$

**TABLE 2. Specific parameters considered for the evaluation of the exposure.**

| Parameters | Symbols | Values | Units |
|---|---|---|---|
| Reference Specific Absorption Rate DL | $SAR_{ref}^{DL}$ | 0.0048 | $\frac{W}{Kg}$ per $\frac{W}{m^2}$ |
| Reference Specific Absorption Rate UL | $SAR_{ref}^{UL}$ | 0.0052 | $\frac{W}{Kg}$ per W |
| TDD duty cycle in UL | $DC_{TDD}^{UL}$ | 0.25 | [-] |
| Time duration in DL [28] | $T^{DL}$ | 3600 | s |
| Time duration in UL [28] | $T^{UL}$ | 35 | s |

With $psSAR_{10g}^{DL}$ the localized SAR obtained similarly to [1], [5] by FDTD simulations using the RT precoded rays (Fig. 1, left) summed over all BS antenna elements as plane wave sources (Fig. 1, middle). Unlike the DL whole-body dose, the DL localized 10g dose is calculated using only the contribution of the serving BS (associated with the users) with precoding.

- Uplink localized 10g dose ($D_{10g}^{UL}$ [J/Kg])
The uplink localized 10g dose is expressed as follows:

$$D_{10g}^{UL} = T^{UL} \cdot psSAR_{10}^{UL} \quad (22)$$

With $T^{UL}$ the duration of exposure to the EMF in seconds [s]; $psSAR_{10g}^{UL}$ the localized 10g SAR caused by the exposure of the user to the uplink transmission of his UE, calculated with the below formula [24]:

$$psSAR_{10g}^{UL} = P_{act} \cdot DC_{TDD}^{UL} \cdot psSAR_{10g}^{ref} \quad (23)$$

where $P_{act}$ is the actual transmission power of the UE obtained as in Eq. 17; $DC_{TDD}^{UL}$ (= 25% [8]) denotes the uplink duty cycle and $psSAR_{10g}^{ref}$ is the reference uplink localized psSAR in [W/Kg] for 1 W of transmitted power ($psSAR_{ref}^{UL} = 22.2$ [W/Kg]), obtained by simulations using the FDTD numerical tool (Sim4life) with a dipole at 3.5 GHz, positioned next to the right ear.

### 3) TRI-OBJECTIVE OPTIMIZATION PROBLEM

As explained earlier in the problem description, two contradicting constraints are accounted for during the optimization: the power consumption and the EMF exposure. We tackle this problem as a tri-objective optimization. In fact, reducing the BS transmit power to limit the EMF exposure yields to a shrinking of the cell's range and therefore many BSs would be required to provide a good coverage of the environment of study, leading to an increase of the total power consumption. In contrary, minimizing the power consumption of the network requires fewer BSs transmitting at higher power. This brings an increase in terms of EMF exposure. So, a good tradeoff is needed to meet the requirements of the mMIMO network. Rather than obtaining a unique solution, the problem requires a set of acceptable trade-optimal solutions.

Thus, the tri-objective optimization problem can be formulated as follows:

$$
\begin{aligned}
P: \max_{\{\boldsymbol{y},\boldsymbol{x},\boldsymbol{p}\}} \quad & \omega_1 f_1 + \omega_2 f_2 + \omega_3 f_3 \\
\text{s.t. } C_1: & \; y_n \in \{0,1\}, \quad \forall n \in \mathcal{N}, \\
C_2: & \; p_n \in \{0,1,2,\cdots,p_t\}, \quad \forall n \in \mathcal{N}, \\
C_3: & \; x_{kn} \in \{0,1\}, \quad \forall n \in \mathcal{N}, \forall k \in \mathcal{K}, \\
C_4: & \; \sum_{k=1}^{K} x_{kn} = 1, \quad \forall n \in \mathcal{N}, \\
C_5: & \; \sum_{j=1}^{3} \omega_j = 1, \\
C_6: & \; \frac{\sum_{n=1}^{N}\sum_{k=1}^{K} x_{kn}}{N} \geq 0.90,
\end{aligned}
$$

where the constraint $C_1$ denotes whether the $n^{th}$ BS is active or not; $C_2$ points out the transmit power of the BS; $C_3$ indicates whether the user $k$ is covered by the BS $n$ or not; $C_4$ shows that a user $k$ can only be connected to one BS $n$; $C_5$ denotes that the weights sum is equal to one [28]. Additionally, the constraint $C_6$ requires the percentage of users served by the active BSs to be above 90%, as per the radio network planning requirements. $\omega_1$, $\omega_2$, $\omega_3$ are the weights indicating the level of priority granted to either objective function.

### E. SCENARIOS AND PROPOSED ALGORITHM

The adopted methodology to optimize the placement of the BSs under the power consumption and EMF exposure constraints relies on relevant use cases inherent to mMIMO system. Specifically, we focus on the enhanced mobile broadband (eMBB) use case whereby a guaranteed throughput of 100 Mbps (on average) [20] is provided to the users regardless of their location. The assumed 100 Mbps data rate complies with the realistic technical requirements, defined by the International Telecommunication Union (ITU [29], [30]), addressing the user experienced data rate in dense areas, for the 5G eMBB use case. The dense suburban area of Ghent and the traffic load at busy hours considered in this study reflect the conditions leading to the assumed user experienced data rate. However, these requirements do not limit the higher performance that might be achieved under other 5G deployments and operating conditions.

The suburban Ghent environment depicted in Fig. 3 is used for the simulation of the different scenarios, based on the capacity network planning tool (right block, Fig. 1).

In this regard, two scenarios have been assumed:

- Scenario 1: the effect of the number of antennas and the number of users on the optimization process is investigated while assuming equal importance of the optimization objectives ($\omega_1 = \omega_2 = \omega_3 = 0.33$). While the number of BS antenna elements is assumed to be 16, 32, 64 or 100, the number of users is derived from the confidential data (daily hourly traffic [12]) provided by a Belgian Mobile operator.
- Scenario 2: the mMIMO network is designed using different optimization weights ($\omega_1 \neq \omega_2 \neq \omega_3$, with $\omega_1 + \omega_2 + \omega_3 = 1$). The Pareto front is discussed to identify optimal solutions. The same assumptions with regards to the number of BS antenna elements and the number of users apply here as well. Furthermore, the results of the

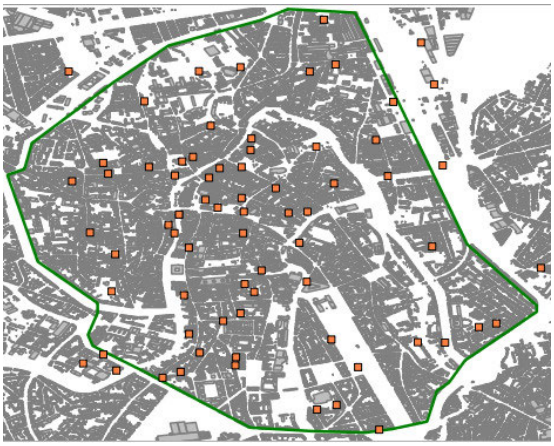

**FIGURE 3.** Ghent outdoor urban environment delimited in green color, where the mMIMO network is deployed. The orange-colored squares indicates the positions of the base stations.

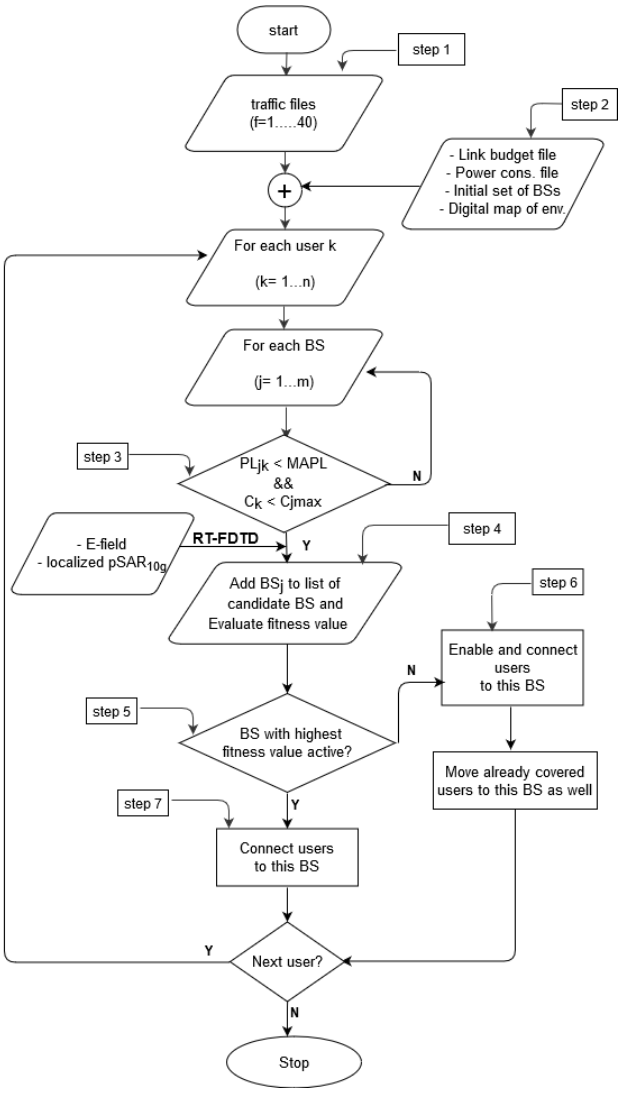


**FIGURE 4.** Proposed optimization algorithm.

simulations obtained from the above scenarios are compared with the reference guidelines recommended by the International Commission for Non-Ionizing Radiation Production (ICNIRP [31], [32]) in terms EMF exposure.

The optimization approach considered in this study is based on system-level simulations for which the initially deployed BSs are successively enabled one at a time in such a way that the demanded user's throughput is guaranteed and the coverage requirement met, with respect to the low power and low EMF exposure constraints. Each time a new BS is enabled, the whole network traffic is balanced between the existing BSs to ensure only the needed ones are retained. The BSs that are not needed resulting from the traffic balance operation are disabled. In the end, the remaining active BSs will form the optimal designed network. The details of the algorithm are explained below. Seven steps are depicted in Fig. 4, that represents the optimization block for the capacity network planner tool in Fig. 1 (right):

- Stage 1: Traffic creation
  - Step 1: Assuming uniform distribution for both the users (within the area of study) and the demanded bit rate, the traffic files are created. These latter contain the user's locations (positions randomly assigned) and their corresponding data rate (64 Kbps and 100 Mbps for the voice and data services, respectively). These files will serve as input for the next step.
- Stage 2: Network calculation
  Here, the design of the optimal network is explained:
  - Step 2: In addition to the traffic files obtained in step 1, supplementary files related to the digital map of the environment of study, the initial set of the 75 BSs provided by the Belgian mobile operator, the link budget parameters and the power consumption values of the individual components of a BS are added. Based on these inputs files, the algorithm proceeds with the optimization of the network and produces output files containing new subsets with fewer base stations, compared to the initial set, accounting for the power consumption and EMF exposure constraints.
  - Step 3: calculate the distance between each user k and the BS $n$ and verify whether the path loss $PL_{nk}$ (calculated with RT) between each user k and the BS $n$ is lower than the maximum allowable path loss (MAPL). At the same time, the BS should afford the demanded capacity of all the users attached to it.
  - Step 4: Make a list of candidate BSs (for users to be associated with) on the basis that the related $PL_{nk}$ is lower than the maximum allowable path loss (MAPL) and the offered maximum capacity ($C_{max}$) can support the data rate demanded by the user (C). For each BS inserted in the list of candidates, calculate the corresponding fitness value based on equation 9, considering the values of the E-Field and the localized $pSAR_{10g}$ calculated by the RT-FDTD tool (Fig. 1, left and middle).
  - Step 5, Sort the BSs inserted in the list of candidate BSs according to their fitness value. The BS with the highest fitness value is assigned to the user k and enabled.
  - Step 6, If there are previously enabled BSs within the network, the algorithm checks the possibility to balance the traffic by transferring covered users to the newly enabled BS unless this latter presents the best the radio conditions (lowest PL). Therefore, any BS emptied by this operation is disabled.
  - Step 7, Go the next user and restart the above steps for all the users spread within the environment study. If no more BSs can be enabled, then the algorithm stops. The resulting set of BSs obtained at the end of the operation constitutes our designed network and the corresponding placements of base stations are considered to be optimal.

In total, 40 simulations (40 times a user distribution) have been run to ensure a good estimation of the parameters of study (number of BSs deployed, power consumption, dose, etc.). The analysis of the results focuses on the 95$^{th}$ percentile.

## III. RESULTS

This section discusses the results of the simulations based on the scenarios presented above. These simulations have been run on a Dell OptiPlex 990 with Intel i5-2400 3.4 GHz processors and 16 GB of RAM. Tables 3 and 4 summarize the main results of the simulations in terms of the 95$^{th}$ percentile of each parameter of interest: the number of BSs required, the power consumption of the obtained network and the EMF exposure (whole-body dose and localized 10g dose).

### A. EQUAL IMPORTANCE OF OPTIMIZATION OBJECTIVES

Here, we consider the same importance between the power consumption and the EMF exposure during the optimization process. In our analysis, this means that $\omega_1 = \omega_2 = \omega_3 = 0.33$.

#### 1) VARYING NUMBER OF USERS

In a first step, the number of BS antennas is fixed, while the number of users is varied to capture its influence over the behavior of the network. So, for each set of 16, 32 and 64 BS antenna elements, we run the simulations for 14, 29, 63, 126, 174, and 224 users, respectively. The number of BS antennas and the maximum number of users are realistic ones obtained from confidential data provided by a mobile GSM operator [12], [19]. The EMF exposure is investigated in terms of doses, consisting of the whole-body downlink dose ($D^{DL}_{wb}$), the whole-body uplink dose ($D^{UL}_{wb}$), the localized 10g dose due to precoding inherent to mMIMO operation in downlink ($D^{DL}_{10g}$) and the localized 10g dose due to the transmissions of the user's devices in uplink ($D^{UL}_{10g}$). These are depicted in Figs. 5, 6, 7, and 8.

**TABLE 3.** Tri-objective optimization: Equal preference of objectives with different number of antennas elements and the number of users ($p_{95}$ = 95th percentile. For the doses, $p_{95}$ applies over 40 simulations of the average/median of the number of users considered for each scenario).

| Scenarios | #BS Ant/#Users | # BS | Power (kW) | $D_{wb}^{DL}$ dose ($p_{95}$) | $D_{wb}^{UL}$ dose ($p_{95}$) | $D_{10g}^{DL}$ dose ($p_{95}$) | $D_{10g}^{UL}$ dose ($p_{95}$) | User Cov. (%) |
|---|---|---|---|---|---|---|---|---|
| $\omega_1 = \omega_2 = \omega_3 = 0.33$ | (-) | $p_{95}$ | $p_{95}$ | $[\frac{mJ}{Kg}]$ | $[\frac{mJ}{Kg}]$ | $[\frac{mJ}{Kg}]$ | $[\frac{J}{Kg}]$ | $p_{95}$ |
| different # users | 64/14 | 11 | 0.72 | 44.7 | 3.61 | 12.2 | 15.41 | 100 |
| | 64/29 | 14 | 0.91 | 59.6 | 4.09 | 4.29 | 17.48 | 100 |
| | 64/63 | 18 | 1.17 | 76.8 | 3.66 | 2.28 | 17.63 | 95.3 |
| | 64/126 | 20 | 1.3 | 89.4 | 4.27 | 1.04 | 18.2 | 92.9 |
| | 64/174 | 21 | 1.32 | 123.6 | 4.44 | 0.64 | 18.98 | 98.4 |
| | 64/224 | 24 | 1.43 | 92.4 | 4.47 | 0.62 | 18.93 | 98.1 |
| different # antennas | 16/224 | 36 | 1.38 | 172 | 4.38 | 0.47 | 18.88 | 95.6 |
| | 32/224 | 28 | 1.21 | 129 | 4.51 | 0.48 | 19.23 | 98.6 |
| | 64/224 | 24 | 1.43 | 92.4 | 4.57 | 0.62 | 18.99 | 98.1 |

**TABLE 4.** Different optimal solutions susceptible to satisfy the low power consumption and low EMF exposure. Scenario with 224 simultaneous active users; 16, 32 and 64 BS antenna elements; $\omega_1 \neq \omega_2 \neq \omega_3$.

| # Ant | Vector | $\omega_1$ | $\omega_2$ | $\omega_3$ | # BS 16 / 32 / 64 / | PC [kW] | Total $D_{wb}$ [J/Kg] | Total $D_{10g}$ [J/Kg] | User Cov. [%] |
|---|---|---|---|---|---|---|---|---|---|
| Best compromise solutions | $V_1$ | 0.33 | 0.33 | 0.33 | 36 / - / - | 1.38 | 0.178 | 14.88 | 95.6 |
| | $V_2$ | 0.4 | 0.2 | 0.4 | 35 / - / - | 1.34 | 0.172 | 15.23 | 95.5 |
| | $V_3$ | 0.6 | 0.2 | 0.2 | 35 / - / - | 1.34 | 0.168 | 16.48 | 95.2 |
| | $V_4$ | 0.2 | 0.4 | 0.4 | - / 28 / - | 1.3 | 0.123 | 17.15 | 97.4 |
| | $V_5$ | 0.7 | 0.1 | 0.2 | - / 28 / - | 1.34 | 0.136 | 17.9 | 99.15 |
| | $V_6$ | 0.5 | 0.5 | 0 | - / - / 23 | 1.44 | 0.088 | 15.87 | 98.28 |
| | $V_7$ | 0.2 | 0.4 | 0.4 | - / - / 22 | 1.43 | 0.088 | 17.73 | 97.4 |

Fig. 5 shows that the $D_{wb}^{DL}$ increases with the number of users served simultaneously at the same time-frequency resource, irrespective of the number of antennas considered at the BS. For instance, with a BS with 64 antenna elements, $D_{wb}^{DL}$ is two times higher when the number of users increases from 14 to 224 users (44.7 [mJ/Kg] with 14 users and 92 [mJ/Kg] with 224 users (Table 3). Given the uniform distribution considered in the analysis, an increase of the number of users would require more BSs to guarantee a better user coverage throughout the network. As a result, there is an increase of the magnitude of the E-field (obtained with the RT) at the location of the users, as the individual complex-conjugated E-fields are summed over all rays and all BSs'antenna elements. Thanks to the control of both the power consumption and the transmit power of the BSs through the optimization process, the number of BSs does not grow indefinitely with the number of served users. This is confirmed in Fig. 5 which shows that the $D_{wb}^{DL}$ increases at a very slow rate when approaching the maximum number of simultaneous served users.

Moreover, besides the whole-body EMF exposure, the localized 10g EMF exposure is investigated. In downlink, the normal mMIMO network operation is characterized by an additional gain at the UE's location due to precoding which gives rise to a localized EMF exposure (here, focus is given to the head) [1], [5]. In this study, the localized downlink 10g dose metric ($D_{10g}^{DL}$) is used to assess this phenomenon. Fig. 6 shows that $D_{10g}^{DL}$ decreases with the number users within the network, irrespective of the size of the mMIMO BS antenna (in terms of antenna elements). As an example, the $D_{10g}^{DL}$ is almost 20 times lower (64 antenna elements, from 12.2 [mJ/Kg] with 14 users and 0.62 [mJ/Kg] with 224 users (Table 3) when the number of active users goes from 14 to 224 users. With the uniform distribution assumed in the study,

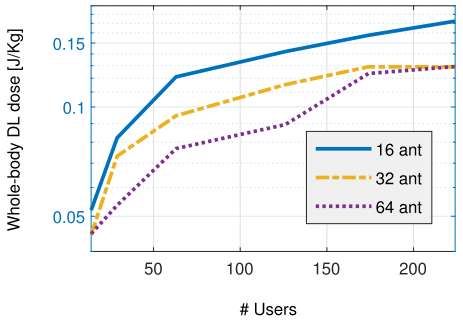


**FIGURE 5.** Whole-body Downlink dose as a function of the number of users simultaneously served in a time-frequency resource.

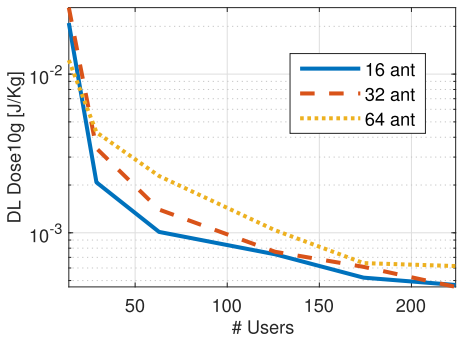


**FIGURE 6.** Downlink localized 10g dose due to precoding as a function of the number of active users, in a time-frequency resource.

the users are widely scattered across the network; so, the total mMIMO BS transmit power is spread across multiple beams to provide coverage to the users, resulting in the reduction of the E-field in each smaller beam.

Focusing on the $D_{wb}^{UL}$ dose in the uplink (Fig. 7), for a fixed number of BS antenna elements, an increase of

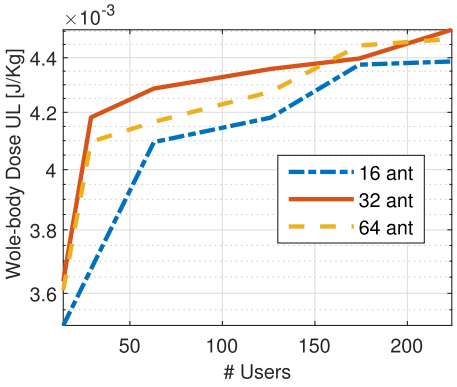


**FIGURE 7.** Whole-body uplink dose as a function of the number of users simultaneously served in a time-frequency resource.

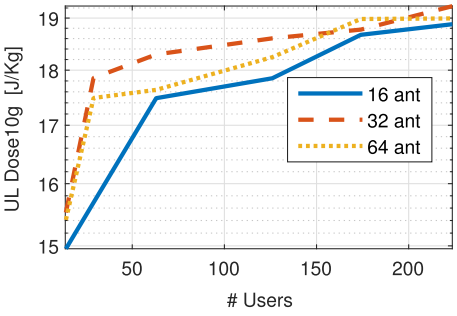


**FIGURE 8.** Uplink localized 10g dose due to transmission of the user's mobile phone as a function of the number of simultaneous active users served in a time-frequency resource.

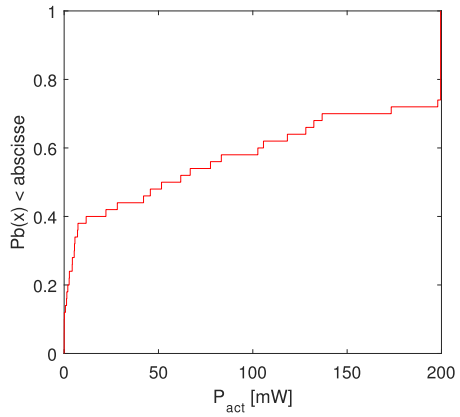


**FIGURE 9.** CDF plot of the user's transmit power. Scenario with equal distribution of optimization objective and a BS with 32 antenna elements serving 224 users.

$D_{wb}^{UL}$ is observed when we vary the number of simultaneous active users in the time-frequency resource. The $D_{wb}^{UL}$ dose increases by 18%, from 3.61 [mJ/Kg] to 4.47 [mJ/Kg], when 64-antenna element BSs are used in the network to serve 14 and 224 users, respectively (Table 3). During the design of the mMIMO network, more BSs will be required to cope with the increase of the number of simultaneous active users. As the BS density increases with the number of active users, the transmit power of the BSs is progressively reduced to meet the optimization constraints related to the low power consumption and low EMF exposure. This results in a deployment of an optimum number of BSs expected to serve the increased number of users. This situation can lead to some users located farther from their serving BS increase their transmit power to avoid any degradation of the signal interference noise ratio (SINR) and the coverage probability. This will maintain a good radio link between the BS and the user. Given that the number of BSs grows with the number of users, the margin of power increase is higher when few users are distributed in the network as the risk of uplink inter-cell interference is very low, compared to the situation where many users are considered. In this latter case, the margin of increasing the transmit power is much more reduced. This explains why in Figs. 7 and 8, similar values of the uplink doses curves are obtained for 224 users while they differ more for lower number of users.

Similarly to $D_{wb}^{UL}$, the $D_{10g}^{UL}$ scales with the number of active users (Fig.8): +23%, from 15.41 [J/Kg] (14 users) to 18.9 [J/Kg] (224 users), when a 64-antenna element BS is used ( Table 3). As explained earlier, the arguments justifying the reason for the increase of the $D_{wb}^{UL}$ (Fig.7) with the number of active users are also applicable here. Fig. 9 shows the distribution of user's transmit power in terms of cumulative distribution function (CDF) for 32 antenna elements and 224 users. It can be noted that the UE's transmit power vary between 0.012 mW and 200 mW (23 dBm) which is the value to not exceed as it refers to the maximum output power for a 5G user's device [26]. In addition, most of the users are transmitting with low power given their closer distance to the serving BS; while some (almost 30%) are transmitting with power higher than 100 mW as they are located farther from the base stations.

When investigating the localized 10g dose, it is noticed that the uplink localized 10g dose $D_{10g}^{UL}$ is the dominant factor and is significantly higher compared to the downlink localized 10g dose $D_{10g}^{DL}$. In a network with 64-antenna element BS, 14 users are exposed to fields resulting in absorbed dose $D_{10g}^{UL}$ of 15.41 J/Kg, while the $Dose_{10g}^{DL}$ is 12.2 mJ/Kg. This is explained by the smaller distance between the user's head and its terminal. In reality, there exists a physical contact with the head of the user, while the BS is located much more further, exposing the signal from the user's terminal to the propagation fadings. The work of [33] ended up with a similar conclusion.

### 2) VARYING THE NUMBER OF BS ANTENNA ELEMENTS

In a second step, the effects of the number of BS antenna elements are investigated (Figs.10 and 11). Fig.10 shows that, for a fixed number of active users, the whole-body downlink Dose ($D_{wb}^{DL}$) reduces as the number of BS antenna elements increases: -46% decrease in terms of $D_{wb}^{DL}$ when the number of antenna elements goes from 16 to 64 (172 [mJ/Kg] for 16-antenna elements and 92.4 [mJ/Kg] for 64-antenna

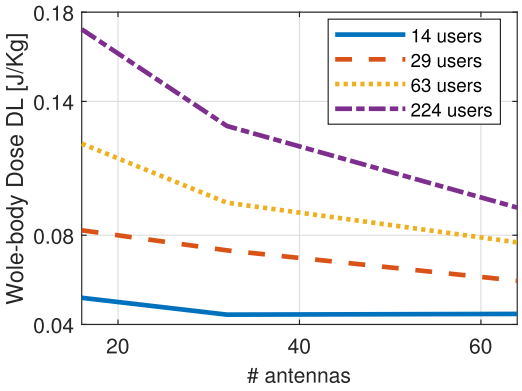


**FIGURE 10.** Whole-body downlink dose due to the transmission of the mMIMO BSs as a function of the number of antenna elements.

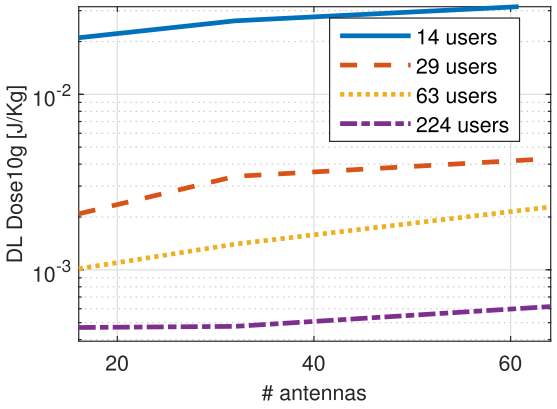


**FIGURE 11.** Downlink localized 10g dose due to precoding or beamforming as a function of the number of antenna elements.

elements with 224 users, Table 3). As explained earlier, the total BS transmit power is equally divided among the antenna elements, resulting in a low DL E-field value per antenna element. In addition, the downlink precoding introduces an additional gain which may increase the range of the cell, resulting in a few number of BSs equipped with many antenna elements. In Table 3, 63% less 64-antenna element BSs are needed to serve 224 users (22 BSs), compared to 16 antenna element BSs (36).

Furthermore, the investigation of the downlink localized 10g dose ($D^{DL}_{10g}$) is depicted in Fig. 11. It can be noticed that the $D^{DL}_{10g}$ scales with the number of BS antenna elements (+31% when the number of antenna elements is expanded from 16 to 64). This is justified by the use of precoding at the BS side, whose gain is proportional to the square root of the number of antenna elements the BS is equipped with [20].

#### 3) POWER CONSUMPTION

In a third step, we investigate the power consumption of the designed network. This is shown in Fig. 12a. When we increase the number of active users from 14 users to 224 users, the power consumption increases as well because the network requires more BSs (Fig. 12b) to provide good coverage

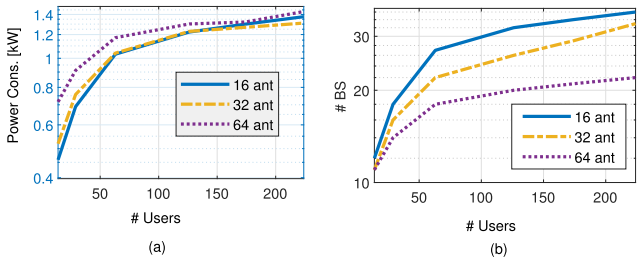


**FIGURE 12.** a. Power consumption of the designed mMIMO networks as a function of the number of active users in the time-frequency resource. b. Number of mMIMO BSs deployed within the environment of study.

to the users distributed across the network. Table 3 shows that 3 times more 16-antenna element BSs (36) are required to serve 224 users, while only 12 16-antenna element BSs are deployed to provide services to 14 users. As a result, the power consumed by the former network is also 3 times higher (1.37 kW for 224 users and 0.46 kW for 14 users). Furthermore, we investigate the influence of the number of BS antenna elements on the power consumption. Fig 12.a shows an upward trend of the power consumed by the network when the number of BS antenna elements increases. This means that the designed network consumes more power when many antenna elements are utilized at the BS. Table 3 shows that the power consumption needed to run a mMIMO network increases by 4% when the antenna elements of its BSs are expanded from 16 to 64 (1.37 kW with 36 16-antenna element BSs vers 1.43 kW with 22 64-antenna element BSs). This is explained by the number of radio-frequency (RF) chains mounted on each BS. There are as many RF chains as number of antenna elements [9]. In addition, the use of combining/precoding schemes in mMIMO necessitates computation complexities that scale with the number of BS antenna elements and requires more power [21], [22].

Another correlation between the number of antenna elements embedded into a mMIMO BS and the number of BSs deployed within the network can be observed in Fig. 12b. The more BS antenna elements, the lower the transmit power per antenna element, resulting in fewer the number of BSs deployed in the network. For instance, in Table 3, there are 22% (28 vs 36 BSs) and 33% (24 vs 36 Bss) less BSs in networks consisting of 32-antenna element BSs and 64-antenna element BSs, respectively, compared to the network with 16-antenna element BSs (Table 3).

### B. BEST COMPROMISE SOLUTIONS

Since the constraints of the optimization problem are conflicting with each other, the solution is not unique; instead, there are several ways of providing reasonable solution vectors that meet the requirements of the optimization, depending on the preference one gives to either objective. Therefore, there is a need to choose the best compromise among the different optimal solutions susceptible to satisfy the low power consumption and low EMF exposure conditions. To realize this, the weighted sum method of the Pareto analysis has been

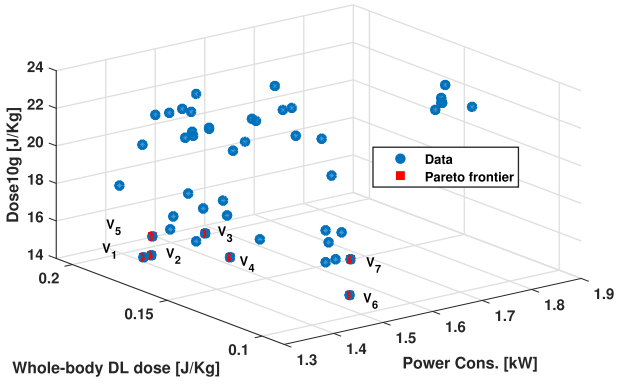


**FIGURE 13.** Pareto frontier ($V_1$ to $V_7$) for the tri-objective optimization problem. Different combinations ($\omega_1; \omega_2; \omega_3$) from 0.1 to 0.9 have been used: 224 simultaneous active users in the time-frequency resource and different BS antenna elements (16, 32, 64).

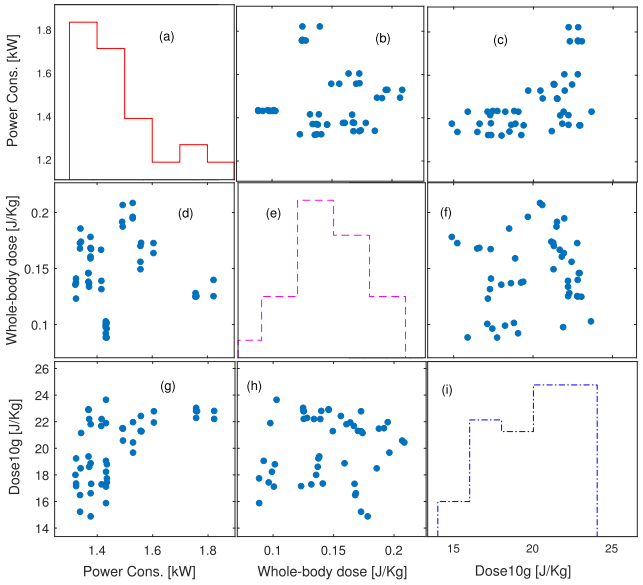


**FIGURE 14.** Pareto set: scatter-plot matrix where the objective functions are pairwise compared in the different subplots. The distributions of each objective function are plotted in the diagonal. Different combinations ($\omega_1; \omega_2; \omega_3$) from 0.1 to 0.9 have been used: 224 simultaneous active users in the time-frequency resource and different BS antenna elements (16, 32, 64).

used to determine the best compromise solution as proposed in [12]. Assuming that the weights $\omega_1$, $\omega_2$, $\omega_3$ randomly take values from 0.1 to 0.9 (such that $\omega_1 + \omega_2 + \omega_3 = 1$), different combinations ($\omega_1; \omega_2; \omega_3$) have been obtained and on the basis of which, we run the simulations using the algorithm described in the above section (Table 4). The values of the power consumption, the total whole-body dose and the total localized 10g dose of each simulated mMIMO scenario have been plotted in Fig. 13, that shows the Pareto frontier corresponding to the best compromise solutions.

Fig. 13 shows the optimal solution vectors in the sense of Pareto indicated in red squared marker, for the worst case scenario when 224 users are distributed within the network. These solution vectors are listed in Table 4. For a better reference in the below discussion, they are numbered from $V_1$ to $V_7$, in their order of appearance in Table 4, from top to down. Depending on the preference of the optimization, one might choose a compromise solution among the seven solution vectors. From a power consumption perspective, the vectors $V_5$ (P = 1.34 kW; $D_{wb}$ = 0.136 J/Kg; $D_{10g}$ = 17.9 J/Kg) corresponding to a network of 28 32-antenna element BSs ($\omega_1 = 0.7; \omega_2 = 0.1; \omega_3 = 0.2$) and $V_4$ (P = 1.32 kW; $D_{wb}$ = 0.123 J/Kg; $D_{10g}$ = 17.15 J/Kg) corresponding to a network of 28 32-antenna element BSs ($\omega_1 = 0.2; \omega_2 = 0.4; \omega_3 = 0.4$) are considered. Both networks present the lowest power consumption values among the different solutions. However, $V_4$ shows a 1.3 % decrease in terms of $D_{wb}$, accompanied by a 4 % increase of $D_{10g}$, compared to $V_4$.

When the focus of the optimization is on the EMF exposure, the networks with 22 64-antenna element BSs ($V_7$: $\omega_1 = 0.2; \omega_2 = 0.4; \omega_3 = 0.4$, P = 1.43 kW; $D_{wb}$ = 0.088 J/Kg; $D_{10g}$ = 17.73 J/Kg) and with 23 64-antenna element BSs ($V_6$: $\omega_1 = 0.5; \omega_2 = 0.5; \omega_3 = 0$, P = 1.44 kW; $D_{wb}$ = 0.088 J/Kg; $D_{10g}$ = 15.87 J/Kg) can be chosen for lower whole-body downlink EMF exposure, while the network with 36 16-antenna element BSs ($V_1$: $\omega_1 = 0.33; \omega_2 = 0.33; \omega_3 = 0.33$, P = 1.38 kW; $D_{wb}$ = 0.178 J/Kg; $D_{10g}$ = 14.88 J/Kg) suits the requirement for the lowest localized 10g EMF exposure. Comparing $V_7$ and $V_1$, the power consumption and $D_{10g}$ are reduced by 3.5% and 6.4 %, respectively, at the expense of $D_{wb}$ which increases by 100%. In the same way, the absorbed energy $D_{10g}$ in $V_6$ is reduced by 6.2 % while the $D_{wb}$ is doubled, in comparison with $V_1$. Among the different solution vectors, the network designed with 27 32-antenna element BSs ($V_6$: $\omega_1 = 0.5; \omega_2 = 0.5; \omega_3 = 0$, P = 1.43 kW; $D_{wb}$ = 0.088 J/Kg; $D_{10g}$ = 14.88 J/Kg) for a power consumption of 1.43 kW, a total whole-body dose of $8.85 \times 10^{-2}$ ($\frac{J}{Kg}$) and a total localized 10g dose of 15.88 J/Kg provides a good compromise.

In Fig. 14, the plot of the Pareto set is shown, allowing a pairwise comparison of the objective functions obtained with 224 users and different BS antenna elements. The histograms in the diagonal correspond to the distribution of the values of the three objective functions: the power consumption (Fig. 14a), the whole-body dose (Fig. 14e) and the localized 10g dose (Fig. 14i) . The comparisons of the different subplots show that the optimum operating windows of the power consumption, the whole-body dose and the localized 10g dose are located at lower values between (1.3 kW to 1.5 kW, Fig. 14b,d), (0.08 J/kg to 0.15 J/kg, Fig. 14f,h) and (14 J/kg to 19 J/kg, Fig. 14c,g), respectively. Beyond these operating windows, the optimization requirements are met simultaneously. When the power consumption is investigated against the the localized 10g dose (Fig. 14c, g), it can be noted that while the $D_{10g}$ is within the operating window, the power consumption points remains relatively constant at low values; but there is an inflection point beyond which an increase of

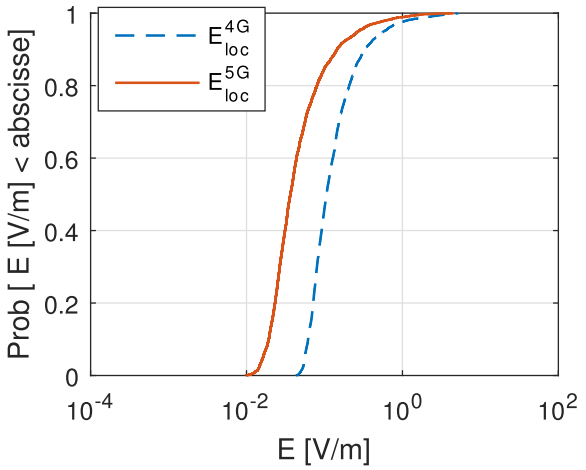


**FIGURE 15.** Cumulative density function comparing the E-field at all locations ( both users and non users ) due to the 4G network and the 5G network designed with the combined RT/FDTD/Network planner method. 64-antenna element BS serving 224 simultaneous active users in the time-frequency resource.

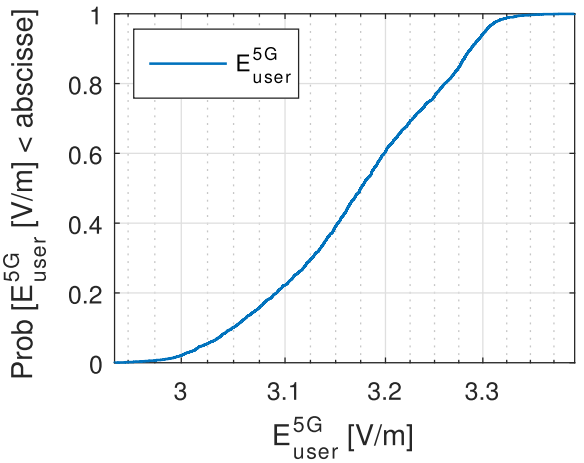


**FIGURE 16.** Cumulative density function of the E-field at the user's location due to the 5G network designed with the combined RT/FDTD/Network planner method. 64-antenna element BS serving 224 simultaneous active users in the time-frequency resource.

power consumption is associated with an increase of $D_{10g}$. This is expected as the increase of the power consumption will lead the BSs to reduce their transmit power for optimization purposes. As a consequence, the UE will slightly increase its uplink power to re-establish the balance of the radio link. Fig. 14h and Fig. 14f show a mixed relationship between the $D_{10g}$ and the $D_{wb}$. Approximately, half of the points are within the $D_{10g}$ operating points, at relatively lower values regardless of the $D_{wb}$. Whereas, the other half with higher $D_{10g}$ values exhibits a downward trend when the $D_{wb}$ increases. A similar behavior is observed when opposing the power consumption to the $D_{wb}$ (Fig. 14b and Fig. 14d). The latter reduces towards lower values when the power consumption grows beyond the operating window. This is the effect of the optimization which imposes the decrease of the $D_{10g}$ and the $D_{wb}$ to meet the requirements of low EMF exposure.

### C. COMPARISON 4G AND 5G E-FIELDS AND LITERATURE

Fig. 15 shows the cumulative distribution function (CDF) to compare the EMF exposure at all locations (containing both users and non-users) due to a 4G LTE network and a mMIMO based 5G network designed with the combined RT/FDTD - Network planning method. The 4G LTE network consists of BSs equipped with a three-sector antenna, each transmitting at 43 dBm, with 10 dBi gain. To ensure a fair comparison of both technologies, the same environment and the same set of initial BSs are utilized for the optimization of the power levels of the antennas and the positions of the BSs. Under equal distribution of the optimization objectives ($\omega_1 = 0.33$; $\omega_2 = 0.33$; $\omega_3 = 0.33$), with a 64-antenna element BS serving 224 users using MRT precoding, the 5G networks designed with the combined RT/FDTD-Network planning tool show a level of E-field almost 2 times lower, compared to the 4G LTE networks: 153 mV/m for 5G massive MIMO network and 339 mV/m for 4G LTE network. This can be explained by the fact that the 4G LTE BS transmits continuously at maximum optimized power, whereas in a mMIMO BS, the transmit power per antenna element is lower due to the multiple antenna elements that equally share the BS transmit power. The authors of [25], [34] ended up with similar conclusions of very low EMF exposure. In [25], the authors successively conducted 5G measurements in the 700 MHz and 3700 MHz frequency bands, over all the locations in Torrino MezzoCammino (TMC), Rome, Italy and showed that the average E-field values vary across the locations and are always pretty low, i.e. lower than 0.9 V/m [25]. [34] proposed an integrated platform to map the residential exposure to radio-frequency EMF sources and showed that the median exposure is very low, almost everywhere in the area of study (0.1-1 V/m), despite very few hotspots with higher exposure (2-2.5 V/m). In the same way, values of time-averaged E-fiels ranging from 288 mV/m to 3.7 V/m have been obtained during in-situ measurements of the exposure due to a 5G NR base station [35].

Fig. 16 shows the distribution of the E-field due to massive MIMO BS at the location of the users, in terms of CDF. The E-field varies from 2.9 V/m to 3.3 V/m. These higher values of the E-field can be explained by (i) the precoding (beamforming) that focuses the beam on the user's location and (ii) the complexity introduced in the combined method that uses the RT tool to calculate the E-field, while including as much as possible the characteristics of the propagation channels in all directions (reflections, transmission and diffraction) [1], [5]. They significantly contribute in the evaluation of a realistic E-field and have an impact on the accuracy of the method. The more complex models are more accurate for the simulations [36]. The measurements carried out in [35], [37], in the 3.4 - 3.8 GHz band obtained E-field values within the same order of magnitude than our study, under continuous data transmission at the vicinity of the user. In [37], with a 64-antenna element BS configuration, different average

E-field strengths have been measured over 6 minutes at the vicinity of the user: 6.5 V/m in Merignac (Huawei Bouygues Telecom), 8.2 V/m in Nozay (Nokia) and 3.9 V/m in Toulouse (Huawei SFR) [37]. In [35], the in-situ measurements of the exposure due to a 5G new radio (NR) mMIMO BS operating at 3.5 GHz lead to time-averaged E-field levels ranging between 288 mV/m (single user scenario) and 3.79 V/m (100% downlink scenario).

Finally, we investigate the compliance of the EMF exposure values obtained in this study with the international guidelines that specifiy quantitative EMF levels for personal exposure. We consider the limits defined in the International Commission for Non-Ioninzing Radion Protection (ICNIRP [31], [32]). For the general public, the above guidelines have set the EMF exposure restrictions to 0.08 W/kg [31], [32] for the whole-body SAR and 2 W/kg [31], [32] for the peak spatial localized SAR averaged over 10g of tissue (Head). From the results of the simulations in Table 3 expressed in terms of dose, we can obtain the corresponding SAR values using the equations in Section II. Thus, a network of 64-antenna element BSs serving 224 users simultaneously (worst case scenario) presents significantly lower EMF exposure values, compared to the international guidelines ($SAR_{10g} = 0.54$ W/kg $\ll 2$ W/kg and $SAR_{wb} = 0.22$ mW/kg $\ll 0.8$ mW/kg).

## IV. CONCLUSION

In this study, we propose an optimization method for the design of multi-cell mMIMO 5G networks with three objectives: the power consumption, the whole-body EMF exposure and the localized 10g EMF exposure (in terms of dose). This method combines the RT-FDTD and the capacity-based deployment tools to account for the spatial consistency requirements of mMIMO which capture all propagation behavior of the environments such as the directional information per antenna element and their inter-correlation. The influence of the number of simultaneous active users and the number of BS antenna elements have been investigated. The simulations show that for a higher number of active users, more BSs are required in the network. As a result, both the whole-body downlink and uplink dose increase with the number of simultaneous active users (+200 % for DL and +18% for UL), while the downlink localized 10g dose reduces (20 times lower) and the uplink localized 10g dose increases (+23%). Furthermore, a design with mMIMO BSs embedding 64 antenna elements results in an increase of the localized 10g downlink dose (+31%) and a decrease of the whole-body downlink dose (−46%), compared to the one with 16-antenna element BSs. Finally, we discuss the accuracy of the new method proposed, in showing that the values of E-field levels obtained with the simulations are in the same order of magnitude than the ones from realistic experiments carried out in different towns. In addition, the 5G E-field strength calculated at all locations with the new method is 2 times lower than the one due to 4G LTE network. Further study will consist of the extension to account for the distributed mMIMO systems where a BS array is divided into sub-arrays, located closer to the users with the objective of mitigating the large-scale fading and improving the spectral efficiency. The EMF exposure due to the bystanders and other users will be investigated as well.

## REFERENCES


[1] S. Shikhantsov, A. Thielens, G. Vermeeren, E. Tanghe, P. Demeester, L. Martens, G. Torfs, and W. Joseph, "Hybrid ray-Tracing/FDTD method for human exposure evaluation of a massive MIMO technology in an industrial indoor environment," *IEEE Access*, vol. 7, pp. 21020–21031, 2019.

[2] Z. Yun and M. F. Iskander, "Ray tracing for radio propagation modeling: Principles and applications," *IEEE Access*, vol. 3, pp. 1089–1100, 2015.

[3] A. I. Sulyman, A. T. Nassar, M. K. Samimi, G. R. Maccartney, T. S. Rappaport, and A. Alsanie, "Radio propagation path loss models for 5G cellular networks in the 28 GHZ and 38 GHZ millimeter-wave bands," *IEEE Commun. Mag.*, vol. 52, no. 9, pp. 78–86, Sep. 2014.

[4] S. Ju and T. S. Rappaport, "Simulating Motion–Incorporating spatial consistency into NYUSIM channel model," in *Proc. IEEE 88th Veh. Technol. Conf. (VTC-Fall)*, Aug. 2018, pp. 1–6.

[5] S. Shikhantsov, A. Thielens, G. Vermeeren, P. Demeester, L. Martens, G. Torfs, and W. Joseph, "Massive MIMO propogation modeling with user-induced coupling effects using ray-tracing and FDTD," *IEEE J. Sel. Areas Commun.*, vol. 38, no. 9, pp. 1955–1963, Sep. 2020.

[6] M. Z. Aslam, Y. Corre, E. Bjornson, and E. G. Larsson, "Large-scale massive MIMO network evaluation using ray-based deterministic simulations," in *Proc. IEEE 29th Annu. Int. Symp. Pers., Indoor Mobile Radio Commun. (PIMRC)*, Sep. 2018, pp. 1–5.

[7] M. Matalatala, M. Deruyck, E. Tanghe, L. Martens, and W. Joseph, "Optimal low-power design of a multicell multiuser massive MIMO system at 3.7 GHz for 5G wireless networks," *Wireless Commun. Mobile Comput.*, vol. 2018, pp. 1–17, Oct. 2018. [Online]. Available: https://www.hindawi.com/journals/wcmc/2018/9796784/

[8] B. Thors, A. Furuskar, D. Colombi, and C. Tornevik, "Time-averaged realistic maximum power levels for the assessment of radio frequency exposure for 5G radio base stations using massive MIMO," *IEEE Access*, vol. 5, pp. 19711–19719, 2017. [Online]. Available: http://ieeexplore.ieee.org/document/8039290/

[9] E. Björnson, J. Hoydis, and L. Sanguinetti, *Massive MIMO Networks* (Foundations and Trends in Signal Processing), vol. 1, no. 1. Hanover, MA, USA: Now Publishers Inc., Nov. 2017.

[10] L. Chiaraviglio, A. S. Cacciapuoti, G. D. Martino, M. Fiore, M. Montesano, D. Trucchi, and N. B. Melazzi, "Planning 5G networks under EMF constraints: State of the art and vision," *IEEE Access*, vol. 6, pp. 51021–51037, 2018.

[11] M. Matalatala, M. Deruyck, E. Tanghe, S. Goudos, L. Martens, and W. Joseph, "Joint optimization towards power consumption and electromagnetic exposure for massive MIMO 5G networks," in *Proc. IEEE 29th Annu. Int. Symp. Pers., Indoor Mobile Radio Commun. (PIMRC)*, Sep. 2018, pp. 1208–1214.

[12] M. Matalatala, M. Deruyck, S. Shikhantsov, E. Tanghe, D. Plets, S. Goudos, K. E. Psannis, L. Martens, and W. Joseph, "Multi-objective optimization of massive MIMO 5G wireless networks towards power consumption, uplink and downlink exposure," *Appl. Sci.*, vol. 9, no. 22, p. 4974, 2019.

[13] Y. Wang, S. Safavi-Naeini, and S. K. Chaudhuri, "A hybrid technique based on combining ray tracing and FDTD methods for site-specific modeling of indoor radio wave propagation," *IEEE Trans. Antennas Propag.*, vol. 48, no. 5, pp. 743–754, May 2000.

[14] M. K. Ozdemir, E. Arvas, and H. Arslan, "Dynamics of spatial correlation and implications on MIMO systems," *IEEE Commun. Mag.*, vol. 42, no. 6, pp. S14–S19, Jun. 2004.

[15] M. Born *et al.*, *Principles of Optics: Electromagnetic Theory of Propagation, Interference and Diffraction of Light*, 7th ed. Cambridge, U.K.: Cambridge Univ. Press, Apr. 2013.

[16] M.-C. Gosselin, E. Neufeld, H. Moser, E. Huber, S. Farcito, L. Gerber, M. Jedensjö, I. Hilber, F. D. Gennaro, B. Lloyd, E. Cherubini, D. Szczerba, W. Kainz, and N. Kuster, "Development of a new generation of high-resolution anatomical models for medical device evaluation: The virtual population 3.0," *Phys. Med. Biol.*, vol. 59, no. 18, pp. 5287–5303, Sep. 2014.

[17] M. T. M. Emmerich and A. H. Deutz, "A tutorial on multiobjective optimization: Fundamentals and evolutionary methods," *Natural Comput.*, vol. 17, no. 3, pp. 585–609, Sep. 2018.
[18] N. Liu, D. Plets, S. K. Goudos, L. Martens, and W. Joseph, "Multi-objective network planning optimization algorithm: Human exposure, power consumption, cost, and capacity," *Wireless Netw.*, vol. 21, no. 3, pp. 841–857, Apr. 2015.
[19] M. Deruyck, E. Tanghe, D. Plets, L. Martens, and W. Joseph, "Optimizing LTE wireless access networks towards power consumption and electromagnetic exposure of human beings," *Comput. Netw.*, vol. 94, pp. 29–40, Jan. 2016.
[20] *Massive MIMO for Efficient Transmission: Deliverables 1.1, Systems Scenarios and Requirements Specifications*, Mammoet, Utrecht, The Netherlands, 2014.
[21] C. Desset, B. Debaillie, and F. Louagie, "Modeling the hardware power consumption of large scale antenna systems," in *Proc. IEEE Online Conf. Green Commun. (OnlineGreenComm)*, Nov. 2014, pp. 1–6.
[22] C. Desset and B. Debaillie, "Massive MIMO for energy-efficient communications," in *Proc. 46th Eur. Microw. Conf. (EuMC)*, Oct. 2016, pp. 138–141.
[23] N. Varsier, D. Plets, Y. Corre, G. Vermeeren, W. Joseph, S. Aerts, L. Martens, and J. Wiart, "A novel method to assess human population exposure induced by a wireless cellular network," *Bioelectromagnetics*, vol. 36, no. 6, pp. 451–463, Sep. 2015.
[24] D. Plets, W. Joseph, K. Vanhecke, G. Vermeeren, S. Aerts, M. Deruyck, and L. Martens, "Whole-body and localized SAR and dose prediction tool for indoor wireless network deployments," in *Proc. 11th Int. Symp. Wireless Commun. Syst. (ISWCS)*, Aug. 2014, pp. 328–332.
[25] L. Chiaraviglio, C. Di Paolo, and N. Blefari-Melazzi, "5G network planning under service and EMF constraints: Formulation and solutions," 2020, *arXiv:2007.16073v1*. [Online]. Available: http://arxiv.org/abs/2007.16073v1
[26] L. Chiaraviglio, A. Elzanaty, and M.-S. Alouini, "Health risks associated with 5G exposure: A view from the communications engineering perspective," 2020, *arXiv:2006.00944*. [Online]. Available: http://arxiv.org/abs/2006.00944
[27] D. Plets, W. Joseph, and L. Martens, *Simulation of Spatial Variations of RF Exposure Within a Macrocell*, vol. 3, no. 3, 2017, pp. 1–2.
[28] P. Ngatchou, A. Zarei, and A. El-Sharkawi, "Pareto multi objective optimization," in *Proc. 13th Int. Conf., Intell. Syst. Appl. Power Syst.*, Nov. 2005, pp. 84–91. [Online]. Available: http://ieeexplore.ieee.org/document/1599245/
[29] *I.T.U. Recommendations: Minimum Requirements Related to Technical Performance for IMT-2020 Radio Interfaces*, I.T.U., Geneva, Switzerland, Oct. 2017.
[30] M. Shafi, A. F. Molisch, P. J. Smith, T. Haustein, P. Zhu, P. De Silva, F. Tufvesson, A. Benjebbour, and G. Wunder, "5G: A tutorial overview of standards, trials, challenges, deployment, and practice," *IEEE J. Sel. Areas Commun.*, vol. 35, no. 6, pp. 1201–1221, Jun. 2017.
[31] I. Commission on Non-Ionizing Radiation Protection (ICNIRP)1, "Guidelines for limiting exposure to electromagnetic fields (100 kHz to 300 GHz)," *Health Phys.*, vol. 118, no. 5, pp. 483–524, May 2020.
[32] International Commission on Non Ionizing Radiation Protection (ICNIRP), "Guidelines for limiting xposure to time-varying electric, magnetic and electromagnetic fields (up to 300 GHz)," *Health Phys.*, vol. 74, no. 4, pp. 494–522, 1998.
[33] S. Kuehn, S. Pfeifer, B. Kochali, N. Kuster, and C. Bern, "Final report: Modelling of total exposure in hypothetical 5G mobile networks for varied topologies and user scenarios," Found. Res. Inf. Technol. Soc. (IT'IS), Tech. Rep., Jun. 2019.
[34] C. Regrain, J. Caudeville, R. de Seze, M. Guedda, A. Chobineh, P. de Doncker, L. Petrillo, E. Chiaramello, M. Parazzini, W. Joseph, S. Aerts, A. Huss, and J. Wiart, "Design of an integrated platform for mapping residential exposure to rf-emf sources," *Int. J. Environ. Res. Public Health*, vol. 17, no. 15, p. 5339, Jul. 2020.
[35] S. Aerts, L. Verloock, M. Van Den Bossche, D. Colombi, L. Martens, C. Tornevik, and W. Joseph, "*In-situ* measurement methodology for the assessment of 5G NR massive MIMO base station exposure at Sub-6 GHz frequencies," *IEEE Access*, vol. 7, pp. 184658–184667, 2019.
[36] R. Pawlak, P. Krawiec, and J. Zurek, "On measuring electromagnetic fields in 5G technology," *IEEE Access*, vol. 7, pp. 29826–29835, 2019.
[37] *Assessment of the Exposure of the General Public to 5G Electromagnetic Waves: First Measurement Results on 5G Pilots in the 3,400-3,800 MHz*, ANFR, Cambo-les-Bains, France, Apr. 2020.

**MICHEL MATALATALA TAMASALA** received the B.Sc. and M.Sc. degrees in applied sciences and electrical engineering from the Polytechnic Faculty of University of Kinshasa, Congo, in 2002 and 2004, respectively. Since 2015, he has been with the Department of Information Technology, Ghent University/IMEC, Ghent, Belgium, where he is currently pursuing the Ph.D. degree in electrical engineering. From 2004 to 2014, he worked for a mobile network operator (MNO) in the Engineering Department, Congo. His research interests include the planning of the next generation massive MIMO-based 5G wireless networks under low power consumption and low EMF exposure constraints, including co-located and distributed architectures.

**SERGEI SHIKHANTSOV** received the B.Sc. and M.Sc. degrees in applied physics and mathematics from the Moscow Institute of Physics and Technology (MIPT), Moscow, Russia, in 2014 and 2016, respectively. He is currently pursuing the Ph.D. degree in engineering physics with Ghent University, Ghent, Belgium.

His research interests include computational electrodynamics, numerical assessment of human electromagnetic field exposure, and propagation modeling of next generation wireless networks.

**MARGOT DERUYCK** was born in Kortrijk, Belgium, in 1985. She received the M.Sc. degree in computer science engineering and the Ph.D. degree from Ghent University, Ghent, Belgium, in 2009 and 2015, respectively. From 2009 to 2015, she was a Research Assistant with IMEC—WAVES (Wireless, Acoustics, Environment, and Expert Systems), Department of Information Technology, Ghent University. Her scientific work is focused on green wireless access networks with minimal power consumption and minimal exposure from human beings. This work led to the Ph.D. degree. She has been a Postdoctoral Researcher with Ghent University, since January 2015, where she continues her work in the green wireless access network. Since October 2016, she has been a Postdoctoral Fellow of the FWO-V (Research Foundation—Flanders).

**EMMERIC TANGHE** (Member, IEEE) was born in Tielt, Belgium, in 1982. He received the M.Sc. and Ph.D. degrees in electrical engineering from Ghent University, Ghent, Belgium, in 2005 and 2011, respectively. From 2005 to 2011, he was a Research Assistant with the Department of Information Technology, Ghent University–imec. His scientific research focused on the modeling of indoor and outdoor propagation through field measurements. In 2015, he became a part-time Professor in medical applications of electromagnetic fields in and around the human body. Since 2011, he has been a Postdoctoral Researcher with Ghent University–imec, where he focuses on propagation modeling. From 2012 to 2018, he was a Postdoctoral Fellow of FWO-V (Research Foundation–Flanders).

**DAVID PLETS** (Member, IEEE) was born in Belgium, in 1983. He received the master's degree in electrotechnical engineering in 2006, with ICT as main subject, and the Ph.D. degree with a dissertation on the characterization and optimization of the coverage of wireless broadcast and WLAN networks. He is currently a member of the WAVES group (Department of Information Technology—INTEC, Ghent University). His current research interests include localization techniques and the IoT, for both industrial and health-related applications. He is also involved in research on optimization of (cognitive) wireless communication networks, with a focus on coverage, interference, and exposure. In October 2016, he became a part-time Professor in exposure to multiple physical agents in smart buildings.

**SOTIRIOS K. GOUDOS** (Senior Member, IEEE) received the B.Sc. degree in physics, the M.Sc. degree in electronics, and the Ph.D. degree in physics from the Aristotle University of Thessaloniki, in 1991, 1994, and 2001 respectively, the Diploma degree in electrical and computer engineering from the Aristotle University of Thessaloniki, in 2011, and the master's degree in information systems from the University of Macedonia, Greece, in 2005.

He joined the Department of Physics, Aristotle University of Thessaloniki, in 2013, where he is currently an Assistant Professor. His research interests include antenna and microwave structures design, evolutionary algorithms, wireless communications, and semantic web technologies. He is a member of the IEICE, the Greek Physics Society, the Technical Chamber of Greece, and the Greek Computer Society. He was an Editor of the book named *Microwave Systems and Applications* (InTech publishers, 2017). He has served as the Technical Program Chair at the International Conference on Modern Circuits and Systems Technologies (MOCAST). He was the Sub-Committee Chair of the Asian-Pacific Microwave Conference (APMC 2017) in the track of smart and reconfigurable antennas. He has also served as a member of the technical program committees in several IEEE and non-IEEE conferences. He is currently serving as an Associate Editor for IEEE Access. He is also a member of the Editorial Board of the *International Journal of Antennas and Propagation (IJAP)*, the *International Journal of Energy Optimization and Engineering*, the *EURASIP Journal on Wireless Communications and Networking*, and the *International Journal on Advances in Intelligent Systems*. He was the Lead Guest Editor of the 2016 and 2017 Special Issues of the IJAP with the topic "Evolutionary Algorithms Applied to Antennas and Propagation: Emerging Trends and Applications." He was also the Lead Guest Editor of the 2018 Special Issue of the *EURASIP Journal on Wireless Communications and Networking* with the topic "Optimization methods for Key Enabling Technologies: 5G, the IoT, and Big Data."

**LUC MARTENS** (Member, IEEE) received the M.Sc. degree in electrical engineering from Ghent University, Ghent, Belgium, in 1986, and the Ph.D. degree in 1990.

From September 1986 to December 1990, he was a Research Assistant with the Department of Information Technology (INTEC), Ghent University, where his scientific work focused on the physical aspects of hyperthermic cancer therapy. His research work deals with electromagnetic and thermal modeling, and the development of measurement systems for that application. Since 1991, he manages the WAVES research group (at the time, the Wireless and Cable research group), INTEC. This group is a part of the IMEC Institute, since 2004. Since April 1993, he has been a Professor with Ghent University. He has authored/coauthored more than 300 publications in the domain of electromagnetic channel predictions, dosimetry, exposure systems and health, and wireless communications. His research interests include modeling and measurement of electromagnetic channels and electromagnetic exposure, e.g., around telecommunication networks and systems, such as cellular base station antennas and energy consumption of wireless networks.

**WOUT JOSEPH** (Senior Member, IEEE) was born in Ostend, Belgium, in October 1977. He received the M.Sc. degree in electrical engineering and the Ph.D. degree from Ghent University, Belgium, in July 2000 and March 2005, respectively.

From September 2000 to March 2005, he was a Research Assistant with the Department of Information Technology (INTEC), Ghent University, where his scientific work was focused on electromagnetic exposure assessment. His research work deals with the measuring and modeling of electromagnetic fields around base stations for mobile communications related to the health effects of the exposure to electromagnetic radiation. Since October 2007, he has been a Postdoctoral Fellow of the FWO-V (Research Foundation—Flanders). Since October 2009, he has been a Professor in the domain of "Experimental characterization of wireless communication systems." He has been a PI of IMEC, since 2017. His professional interests include electromagnetic field exposure assessment, propagation for wireless communication systems, antennas, and calibration. Furthermore, he specializes in wireless performance analysis and Quality of Experience.